Measurement of Off-Axial Aberration

IOP Conf. Series: Journal of Physics: Conf. Series **902** (2017) 012011 doi:10.1088/1742-6596/902/1/012011

Measurement of Off-Axial Aberration

Hidetaka Sawada[1,2,3], and Angus I. Kirkland[1,2]

[1]ePSIC: Electron Physical Sciences Imaging Centre, Diamond Light Source Ltd, Didcot, Oxford, OX11 0DE, UK
[2]Department of Materials, University of Oxford, Parks Road, Oxford OX1 3PH, UK
[3]JEOL UK Ltd., Silver Court Watchmead Welwyn Garden City, Herts.,AL7 1LT, UK

E-mail: hide.sawada@materials.ox.ac.uk

Abstract. High-resolution observation of a large field of view with a high quality detector is important for single particle analysis or in-situ experiments. Consequently, evaluation of aberrations that depend on position in the field of view, (off-axial aberrations) is required. We report the experimental measurement of off-axial aberrations including higher order components in several optical conditions together with the corresponding off-axial phase maps.

1. Introduction

Owing to the development of a high quality cameras with a large number of pixels, high resolution observations in both materials science and life science over a large field of view is becoming important in transmission electron microscopy (TEM). Atomic-resolution observation of two-dimensional materials and in-situ studies in the TEM require optimization of the electron-optical conditions over a large field of view, for example to understand point defects, dislocations and distortions of the lattice [1]. High-resolution image recording for single particle analysis with wide field of view cameras is also necessary to image a suitably large number of particles for reconstruction. However, when recording high-resolution TEM data with a large field of view, off-axial aberrations increase in the peripheral area, corrupting the data. Consequently, high-quality imaging is guaranteed only at the center axis of the image. Evaluation of off-axial aberrations is hence required to optimize the optical conditions for wide field of view imaging.

Measurement of off-axial aberrations using diffractogram from different positions in the experimental image field of view has been previously reported [2]. In this study, we define the off-axial aberrations, and extend the measurement of these to defocus and two-fold astigmatism up to 4th rank. Features arising from of off-axial aberrations are discussed using the simulated patterns of diffractograms and compared to experimental measurements using an off-axial aberration phase map.

2. Measurement of off-axial aberrations

Aberrations including a spatial vector, $\mathbf{r} = (x, y)$ are defined as off-axial aberrations (Fig.1(b)), whereas aberrations that are described by only a complex angle, $\boldsymbol{\omega} = \boldsymbol{\alpha} \cdot \mathbf{exp}(\mathbf{i}\boldsymbol{\theta})$ are defined as axial aberrations (Fig.1(a)), where α is the amplitude of the angle and θ is the azimuth. The total wave aberration function, $\boldsymbol{W_{total}}$ is described by summation of the axial and off-axial aberrations, as;

$$\boldsymbol{W}_{total} = \boldsymbol{W}_{axial} + \boldsymbol{W}_{off\ axial} \quad (1)$$

where $\boldsymbol{W}_{axial}$ is the axial wave aberration function and $\boldsymbol{W}_{off\ axial}$ is the off-axial wave aberration function.

The axial wave aberration function can be rewritten as;

$$\boldsymbol{W}_{axial} = \sum_{m,n} \frac{1}{m+n} \mathrm{Re}(\boldsymbol{C}_{m,n} \bar{\boldsymbol{\omega}}^m \boldsymbol{\omega}^n) \quad (2)$$

where $\bar{\boldsymbol{\omega}} = \alpha \cdot \exp(-i\theta)$ is the complex conjugate of $\boldsymbol{\omega}$.

The off-axial aberration wave function is given by;

$$\boldsymbol{W}_{off\ axial} = \sum_{m,n,s,t} \frac{1}{m+n} \mathrm{Re}\left(\boldsymbol{K}_{m,n,s,t} \bar{\boldsymbol{\omega}}^m \boldsymbol{\omega}^n \bar{\boldsymbol{r}}^s \boldsymbol{r}^t\right) \quad (3)$$

where $\mathbf{r} = |r| \cdot \exp(i\theta_r)$ is a complex position, $|r|$ is amplitude of the complex position and θ_r is the azimuth of the complex position. In order to extend measurements to higher orders of off-axial aberration coefficients, a dimensionless parameter can be conveniently introduced to give the same unit for all coefficients. Hence, a dimensionless angle, $\boldsymbol{\gamma}$ is introduced as a parameter for the spatial position and consequently the off axial wave aberration function, $\boldsymbol{W}_{off\ axial}$ can be rewritten as;

$$\boldsymbol{W}_{off\ axial} = \sum_{m,n,s,t} \frac{1}{m+n} \mathrm{Re}\left(\boldsymbol{K}_{m,n,s,t(r0)} \bar{\boldsymbol{\omega}}^m \boldsymbol{\omega}^n \bar{\boldsymbol{\gamma}}^s \boldsymbol{\gamma}^t\right) \quad (4)$$

where the complex dimensionless position $\boldsymbol{\gamma}$ at r_0; r_0 is a standard length; $\boldsymbol{\gamma} = |\gamma| \cdot \exp(i\theta_\gamma)$ with $|\gamma| = |r|/|r_0|$, which is the amplitude of the complex dimensionless position and $\theta_\gamma = \theta_r$ is the azimuth of the complex position. The geometrical order, N of the axial aberrations is $N = m + n - 1$, and R is a rank including the off-axial aberrations with $R = N + s + t$ [3]. The off-axial aberration coefficient of $\boldsymbol{K}_{m,n}$ at r_0 for an axial aberration $\boldsymbol{C}_{(m+n)}$ can be described by summation of each rank of the off-axial aberrations as,

$$\boldsymbol{K}_{m,n} = \sum_{s,t} \boldsymbol{K}_{m,n,s,t(r0)} \bar{\boldsymbol{\gamma}}^s \boldsymbol{\gamma}^t \quad (5)$$

Hence, each coefficient (vector) of the off-axial aberrations for $(m, n, s. t)$ at $r_0$is the term corresponding to complex position of $\bar{\boldsymbol{\gamma}}^s \boldsymbol{\gamma}^t$ defined as $\boldsymbol{K}_{m,n,s,t(r0)}$. For the data reported, $\boldsymbol{\gamma}$ is defined at r_0=100 nm whence an off axial aberration coefficient corresponds to a value of the axial aberration 100 nm away from the centre of the axial position with a unit of length in this case.

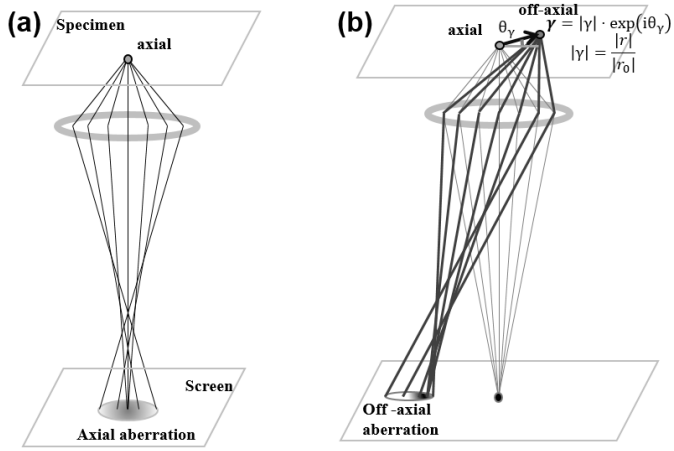

Figure 1. (a) Schematic diagram of (a) axial aberrations. (b) off-axial aberrations.

Table 1: Off-axial aberration coefficients. Using corresponding axial aberration notations, $\mathbf{O_2}$ denotes defocus, $\mathbf{A_2}$ denotes two-fold astigmatism, $\mathbf{P_3}$ denotes axial coma, and $\mathbf{A_3}$ denotes three-fold astigmatism.

	Off-axial aberration $\boldsymbol{K}_{m,n,s,t(r0)}$			
Axial aberration	Off-axial aberration	2nd rank	3rd rank	4th rank
$\mathbf{O_2}$	$\mathrm{Re}[\boldsymbol{O}_{2\,\bar{\gamma}^s\gamma^t{}_{(r0)}}]$	$\mathbf{O}_{2\,\gamma_{(r0)}}$	$\mathbf{O}_{2\,\gamma\bar{\gamma}_{(r0)}}$, $\mathbf{O}_{2\,\gamma^2{}_{(r0)}}$	$\mathbf{O}_{2\,\gamma^2\bar{\gamma}_{(r0)}}$, $\mathbf{O}_{2\,\gamma^3{}_{(r0)}}$
$\mathbf{A_2}$	$\boldsymbol{A}_{2\,\bar{\gamma}^s\gamma^t{}_{(r0)}}$	$\mathbf{A}_{2\,\gamma_{(r0)}}$, $\mathbf{A}_{2\,\bar{\gamma}_{(r0)}}$	$\mathbf{A}_{2\,\gamma\bar{\gamma}_{(r0)}}$, $\mathbf{A}_{2\,\gamma^2{}_{(r0)}}$, $\mathbf{A}_{2\,\bar{\gamma}^2{}_{(r0)}}$	
$\mathbf{P_3}$	$\boldsymbol{P}_{3\,\bar{\gamma}^s\gamma^t{}_{(r0)}}$		$\mathbf{P}_{3\,\gamma_{(r0)}}$, $\mathbf{P}_{3\,\bar{\gamma}_{(r0)}}$	
$\mathbf{A_3}$	$\boldsymbol{A}_{3\,\bar{\gamma}^s\gamma^t{}_{(r0)}}$		$\mathbf{A}_{3\,\gamma_{(r0)}}$, $\mathbf{A}_{3\,\bar{\gamma}_{(r0)}}$	

Table 2: Coefficients of off-axial defocus and off-axial two-fold astigmatism

Symmetry → Rank ↓	0	1	2	3	0	1	2	3	4
	Off-axial defocus				Off-axial two-fold astigmatism				
2		$\mathbf{O}_{2\,\gamma_{(r0)}}$				$\mathbf{A}_{2\,\gamma_{(r0)}}$		$\mathbf{A}_{2\,\bar{\gamma}_{(r0)}}$	
3	$\mathbf{O}_{2\,\gamma\bar{\gamma}_{(r0)}}$		$\mathbf{O}_{2\,\gamma^2{}_{(r0)}}$		$\mathbf{A}_{2\,\gamma^2{}_{(r0)}}$		$\mathbf{A}_{2\,\gamma\bar{\gamma}_{(r0)}}$		$\mathbf{A}_{2\,\bar{\gamma}^2{}_{(r0)}}$
4		$\mathbf{O}_{2\,\gamma^2\bar{\gamma}_{(r0)}}$		$\mathbf{O}_{2\,\gamma^3{}_{(r0)}}$					

Diffractograms at different positions in a field of view were simulated using second rank off-axial defocus and off-axial two-fold astigmatism (Fig.2). Figure 2(a) shows diffractograms of segmented areas from the full field of view with off-axial defocus, $\mathbf{O}_{2\,\gamma_{(100nm)}}$ = (100nm,0) and axial defocus, $\mathbf{O}_2$ = –100 nm. The defocus with position in the field of view is determined by the off-axial defocus and the defocus becomes close to zero at the right hand side. Figure 2(b) shows diffractograms from segmented areas with $\mathbf{O}_{2\,\gamma_{(100nm)}}$ =(0,100nm), where the defocus at the lower part is close to zero. The position dependence of defoci due to the off-axial defocus $\mathbf{O}_{2\,\gamma_{(100nm)}}$ = (0,100nm) shows a 90° rotation relationship to the off-axial defocus $\mathbf{O}_{2\,\gamma_{(100nm)}}$ =(100nm,0). Figs. 2(c) and 2(d) show diffractograms from segmented areas with off-axial two-fold astigmatism, $\mathbf{A}_{2\,\gamma}$ and $\mathbf{A}_{2\,\bar{\gamma}}$, respectively. The two-fold astigmatism becomes larger toward the edge of the field of view, and the azimuth of the two-fold astigmatism changes depending on position. A map of $\mathbf{A}_{2\,\bar{\gamma}}$ shows an overall three-fold symmetry, since the symmetry of the pattern in the field of view is |(m-n) + (s-t)| in the case of off-axial defocus and off-axial two-fold astigmatism. Table 3 lists examples of measured coefficients for the off-axial aberrations using experimental diffractograms at a 200kV using JEM-ARM300F.

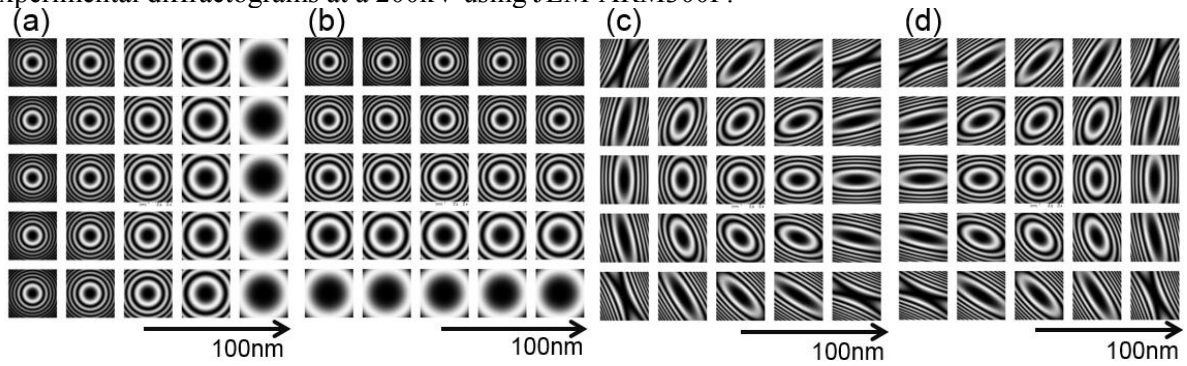

Figure 2. Diffractograms from segmented areas with a width of 200 nm (a)$\mathbf{O}_{2\,\gamma_{(100nm)}}$ = (100nm,0), (b) $\mathbf{O}_{2\,\gamma_{(100nm)}}$ = (0,100nm), (c) $\mathbf{A}_{2\,\gamma_{(100nm)}}$ = (100nm, 0) (d) $\mathbf{A}_{2\,\bar{\gamma}_{(100nm)}}$ = (0, –100nm).

Table 3. Measured values of off axial aberration coefficients. (r_0=100 [nm])

Rank	Off-axial aberration	Amplitude	Azimuth	Rank	Off-axial aberration	Amplitude	Azimuth
2	$O_{2\,\gamma_{(r0)}}$	8.620 nm	–102.00°	2	$A_{2\,\gamma_{(r0)}}$	1.9067 nm	–156.65°
3	$O_{2\,\gamma\bar{\gamma}_{(r0)}}$	–0.3148 nm		2	$A_{2\,\bar{\gamma}_{(r0)}}$	1.1012 nm	–18.94°
3	$O_{2\,\gamma^2{}_{(r0)}}$	0.4245 nm	–24.02°	3	$A_{2\,\gamma^2{}_{(r0)}}$	0.7866 nm	165.90°
4	$O_{2\,\gamma^2\bar{\gamma}_{(r0)}}$	0.1341 nm	177.86°	3	$A_{2\,\gamma\bar{\gamma}_{(r0)}}$	0.5034 nm	12.55°
4	$O_{2\,\gamma^3{}_{(r0)}}$	0.0264 nm	–67.50°	3	$A_{2\,\bar{\gamma}^2{}_{(r0)}}$	0.5401 nm	–92.60°
3	$P_{3\,\gamma_{(r0)}}$	407.66 nm	–30.10°	3	$A_{3\,\gamma_{(r0)}}$	5.963 nm	61.76°
3	$P_{3\,\bar{\gamma}_{(r0)}}$	50.907 nm	–77.95°	3	$A_{3\,\bar{\gamma}_{(r0)}}$	13.317 nm	154.36°

3. Experimental measurement of off-axial aberrations

Figs. 3(d-f) show off-axial phase maps from experimental measurements. Figs.3(a-c) were recorded by changing the excitation of the transfer lens (TL) between two multipoles in the TEM corrector. Fig.3(a)

was recorded using a weaker excitation of the TL, and Fig.3(c) with a stronger excitation. The TL excitation used to record Fig.3(b) is intermediate between that used to record Figs.3(a) and 3(c). In general, specimen or local bending introduces a defocus change across the field of view, artificially resulting in second rank off-axial defocus. To distinguish genuine electron-optical off-axial aberrations from this specimen effect, the second rank off-axial defocus was set to zero in the phase maps shown in Figs.3(d-f). From these measurements, the value of a $A_{2\bar{\gamma}}$, which has three-fold symmetry, shows a significant difference (Table 4). The off-axial aberrations cause a change of the two-fold astigmatism at the periphery of the field of view demonstrating that optimization of $A_{2\,\bar{\gamma}}$ is important for a double hexapole TEM corrector.

Table 4: Measured values of off axial aberrations. (r_0=100 [nm])

	Setting 1(Figs.3(a) and 3(d))		Setting 2(Figs.3(b) and 3(e))		Setting 3(Figs.3(c) and 3(f))	
Off-axial aberration	Amplitude	Azimuth	Amplitude	Azimuth	Amplitude	Azimuth
$A_{2\,\gamma_{(r0)}}$	1.81 nm	142.59°	1.83 nm	–125.38°	2.67 nm	–110.61°
$A_{2\,\bar{\gamma}_{(r0)}}$	**4.38** nm	72.71°	**1.04** nm	101.96°	**2.70** nm	–131.97°

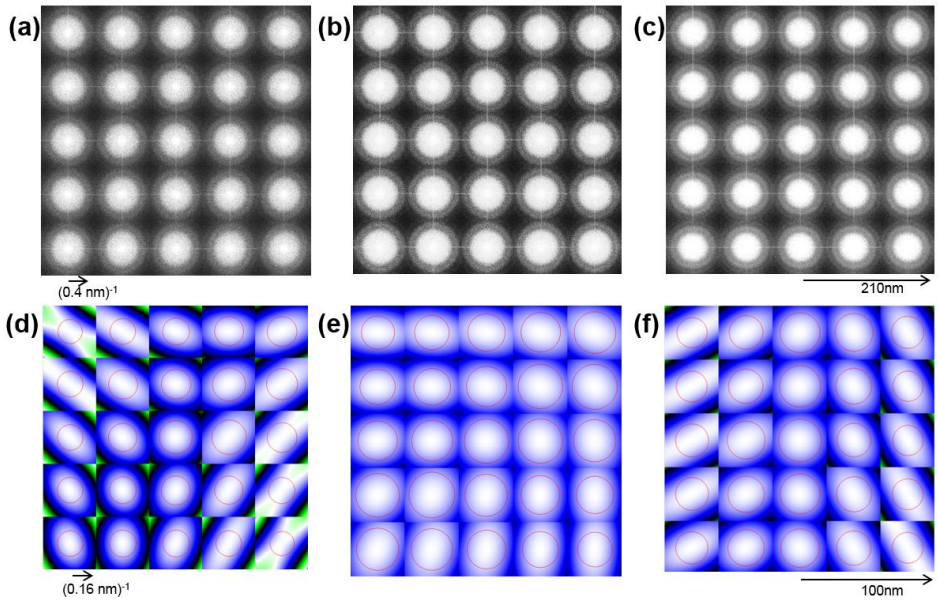

Figure 3. (a-c) 5x5 diffractogram maps from segmented areas. (d-f) Off-Axial Phase Map for different TL excitations. An offset, O_2= –5 nm is used to visualize the off-axial two-fold astigmatism in the phase maps. Red circles denote the $\pi/4$ phase limit within each local area.

4. Conclusion

Measurement of off-axial aberrations including those of higher rank was reported using diffractograms calculated from different positions in a wide field of view. Experimental measurements have been reported for several optical settings. For the measurements reported off-axial two-fold astigmatism, $A_{2\bar{\gamma}}$, with a three-fold symmetry across the field of view is clearly evident in images recorded using a double-hexapole TEM corrector.

References

[1] Warner J H, Margine E R, Mukai M, Robertson A W, Giustino F and Kirkland A I 2012 *Science* **337** 209-212.
[2] Maßmann I, Uhlemann S, Müller H, Hartel P, Zach J, Haider M, Taniguchi Y, Hoyle D and Herring E 2011 *Microsc. Microanal.* **17** Suppl. 1270.
[3] Hawkes P W and Kasper E 1989 Principles of Electron Optics. Academic Press. London. UK.